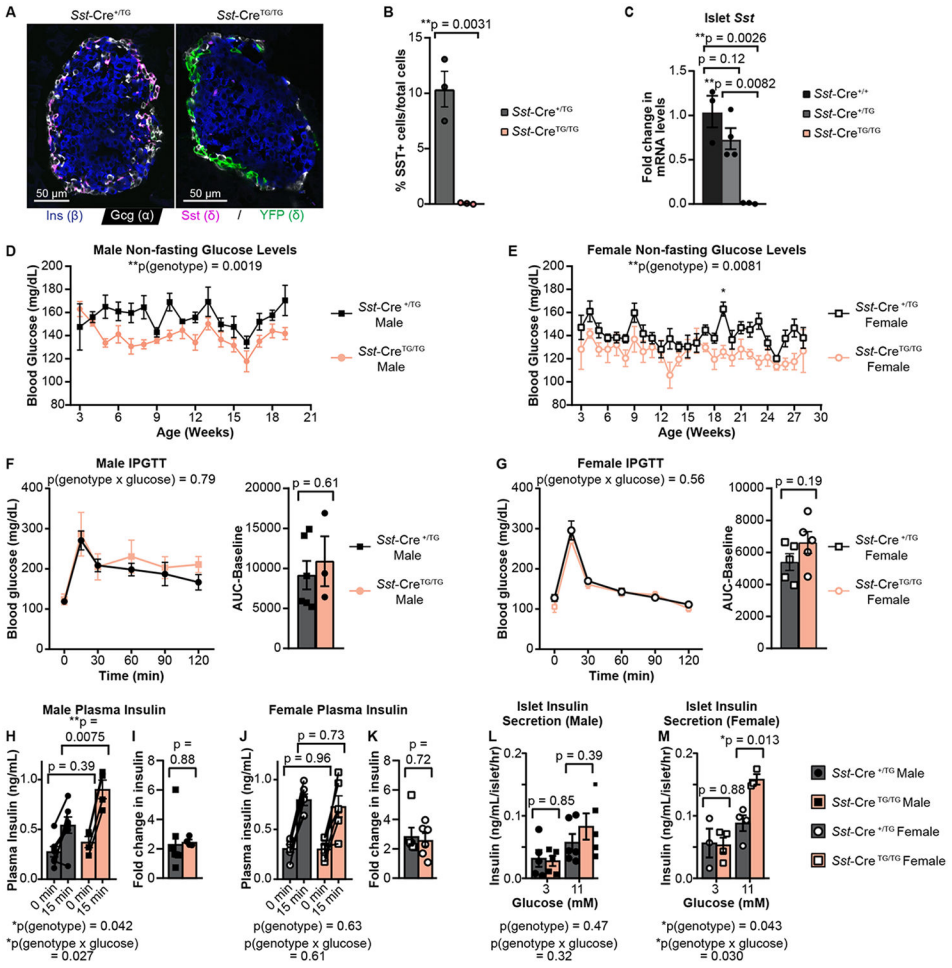

Fig. 1. *Sst*-Cre$^{TG/TG}$ mice exhibit loss of *Sst* and a decreased glycemic set point.

A) Immunofluorescent stain of pancreas section from a *Sst*-Cre$^{+/TG}$ x lsl-YFP (left) and *Sst*-Cre$^{TG/TG}$ x lsl-YFP mouse (right). B) Quantification of SST+ cell number (n=3 *Sst*-Cre$^{+/TG}$, n=3 *Sst*-Cre$^{TG/TG}$). C) *Sst* mRNA levels in islets from *Sst*-Cre$^{+/+}$ (n=3), *Sst*-Cre$^{+/TG}$ (n=4), and *Sst*-Cre$^{TG/TG}$ (n=3) mice. D and E) Weekly blood glucose measurements of male (D, n=6 *Sst*-Cre$^{+/TG}$, n=9 *Sst*-Cre$^{TG/TG}$) mice and female (E, n=7 *Sst*-Cre$^{+/TG}$, n=7 *Sst*-Cre$^{TG/TG}$) mice, grouped by age. F and G) Glucose tolerance and quantification of the AUC-baseline of male (F, n=6 *Sst*-Cre$^{+/TG}$, n=3 *Sst*-Cre$^{TG/TG}$) and female (G, n=5 *Sst*-Cre$^{+/TG}$, n=5 *Sst*-Cre$^{TG/TG}$) mice. H) Plasma insulin levels before and 15 min after IP glucose administration in male mice (n=5 *Sst*-Cre$^{+/TG}$, n=4 *Sst*-Cre$^{TG/TG}$). I) Fold change in plasma insulin levels of male mice in H. J) Plasma insulin levels before and 15 min after IP glucose administration in female mice (n=6 *Sst*-Cre$^{+/TG}$, n=6 *Sst*-Cre$^{TG/TG}$). K) Fold change in plasma insulin levels of female mice in J. L and M) Static insulin secretion assay using islets from male (L, n=6 replicates, 10 islets each, pooled from 5 *Sst*-Cre$^{+/TG}$ or 4 *Sst*-Cre$^{TG/TG}$ mice) and female (M, n=4 replicates, 10 islets each, pooled from 6 *Sst*-Cre$^{+/TG}$ or 6 *Sst*-Cre$^{TG/TG}$ mice) mice incubated at 3 mM glucose and 11 mM glucose. Significance was determined by two-tailed unpaired t-test (B, AUC for F and G, I, K), one-way ANOVA followed by Holm-Sidak's adjustment for multiple comparisons (C), and two-way ANOVA or mixed modeling for genotype and time (D and E) or genotype and

glucose (F, G, H, J, L, M) followed by comparison of individual points by Holm-Sidak's adjustment multiple comparisons (E: *p=0.027). Error bars represent SEM.

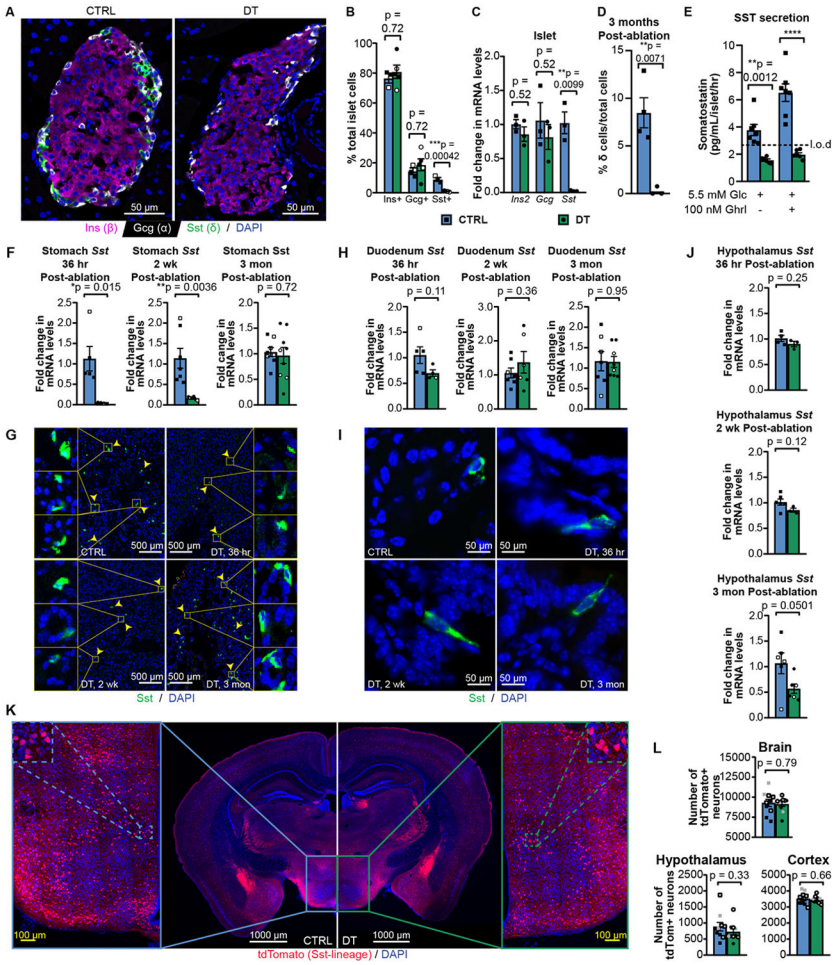

Fig. 2. Specific ablation of pancreatic δ cells in *Sst*-Cre x lsl-DTR mice.

A) Pancreas sections from control (CTRL) and δ cell-ablated (DT) mice. Scale bar represents 50 μm. B) Insulin, glucagon, and SST+ cell quantification (n=3 CTRL, n=5 DT). C) *Ins2, Gcg,* and *Sst* mRNA levels in islets from CTRL (n=3) and DT (n=3) mice. D) SST+ cell quantification 3 months post-ablation (n=4 CTRL, n=3 DT). E) SST secretion from CTRL (n=7 replicates, 30 islets each, pooled from 4 mice) and DT islets (n=6 replicates, 30 islets each, pooled from 4 mice) in 5.5 mM glucose +/− 100 nM ghrelin; l.o.d. = limit of detection. F and G) *Sst* mRNA levels (F) and SST stain (G) in stomach tissue collected 36 hours (n=5 CTRL, n=4 DT), 2 weeks (n=7 CTRL, n=6 DT), or 3 months (n=8 CTRL, n=9 DT) post-treatment. Yellow arrows indicate gastric D cells; yellow boxes indicate close-ups. Scale bars represent 500 μm. H and I) *Sst* mRNA levels (H) and SST stain (I) in duodenum tissue collected 36 hours (n=5 CTRL, n=4 DT), 2 weeks (n=7 CTRL, n=5 DT), or 3 months (n=7 CTRL, n=8 DT) post-treatment. J) *Sst* mRNA levels in hypothalamus collected 36 hours (n=4 CTRL, n=3 DT), 2 weeks (n=6 CTRL, n=3 DT), or 3 months (n=6 CTRL, n=6 DT) post-treatment. K) Brain cross-sections collected from *Sst*-Cre x lsl-tdTomato mice with (DT) or without lsl-DTR (CTRL) 36 hours post-DT, with close-ups of the hypothalamus region on the sides and further close-ups of neurons in the top corners. L) tdTomato+ neuron quantification in brain, hypothalamus, and cortex. 10 images from N=3 mice per group (represented by a black, gray, or open symbol) were quantified. Closed symbols

represent males and open symbols represent females in graphs. Significance was determined by multiple two-tailed unpaired t-tests followed by Holm-Sidak correction (B, C), two-tailed unpaired t-test (D, F, H, J, L), or two-way ANOVA followed by Holm-Sidak correction (E, ****p<0.0001). Error bars represent SEM.

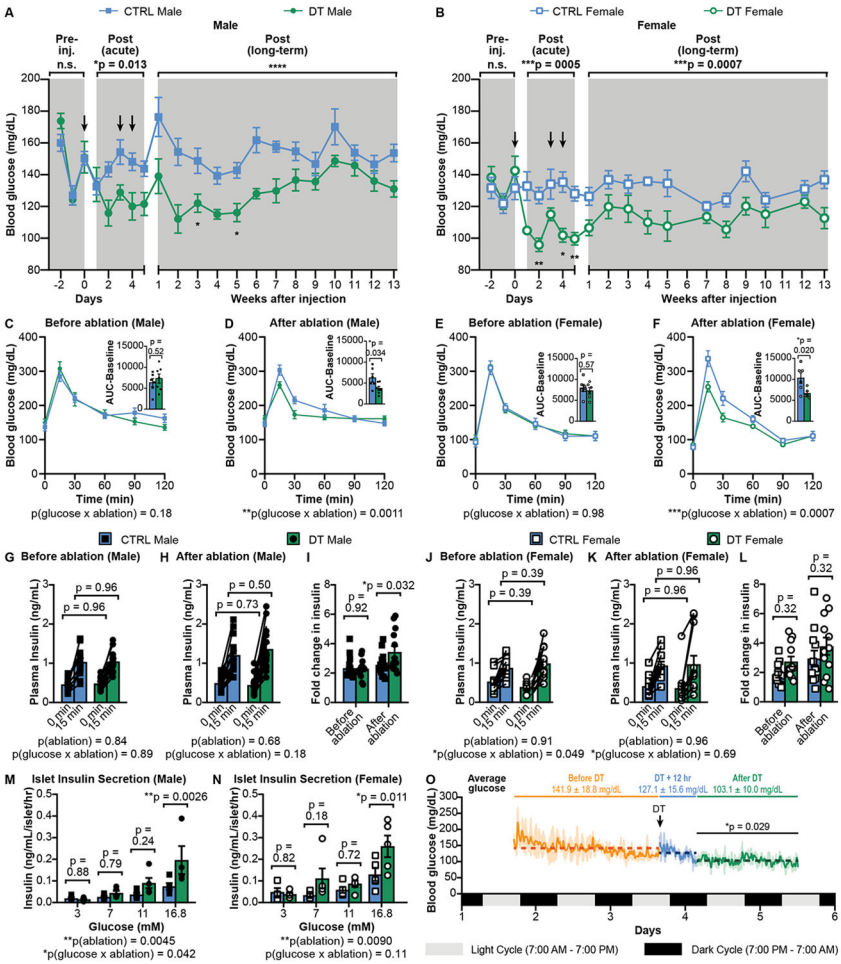

Fig. 3. δ cell ablation decreases the glycemic set point and increases glucose tolerance and insulin secretion.

A and B) Blood glucose measurements of male (A, n=8 CTRL, n=6 DT) and female (B, n=6 CTRL, n=6 DT) mice. Black arrows represent IP administration of SAL or DT. C-F) GTT of male mice (C-D: n=6 CTRL, n=7 DT) C) before and D) after δ cell ablation, and female mice (E-F: n=6 CTRL, n=6 DT) E) before and F) after δ cell ablation. Bar graphs in the upper right-hand corner of each line graph represent AUC-baseline. G-H) Plasma insulin measurements in male mice (n=15 CTRL, n=13 DT) G) before and H) after ablation. I) Fold change in plasma insulin levels between male CTRL and DT mice from G-H before and after ablation. J-K) Plasma insulin measurements in female mice (n=12 CTRL, n=12 DT) J) before and K) after ablation. L) Fold change in plasma insulin levels between female CTRL and DT mice from J-K before and after ablation. M and N) Static insulin secretion assay performed on islets isolated from ablated M) male (n=5 replicates per group, 10 islets each, pooled from 3 CTRL or 3 DT mice) and N) female (n=5 replicates per group, 10 islets each, pooled from 3 CTRL or 3 DT mice) mice. O) Averaged CGM data from n=3 mice. Orange represents glucose levels prior to single IP injection of DT. Blue represents when DT was administered and the 12 hours following. Green represents glucose levels measured 12 hours post-DT administration until the end of the experiment. Dashed lines represent average glucose level throughout each time period. Shaded regions around the line graph represent

SD. Significance was determined by two-way ANOVA for ablation (A, ****p<0.0001; B) or ablation and glucose (C-N, I, M, N) followed by Holm-Sidak's correction for multiple comparisons (A: *p=0.026, *p=0.039; B: **p=0.0057, *p=0.012, **p=0.0057), two-tailed unpaired t-test for AUC-baseline (C-F) or a one-way ANOVA of average glucose at baseline, DT, and after DT followed by Holm-Sidak's correction (O). Error bars represent SEM.

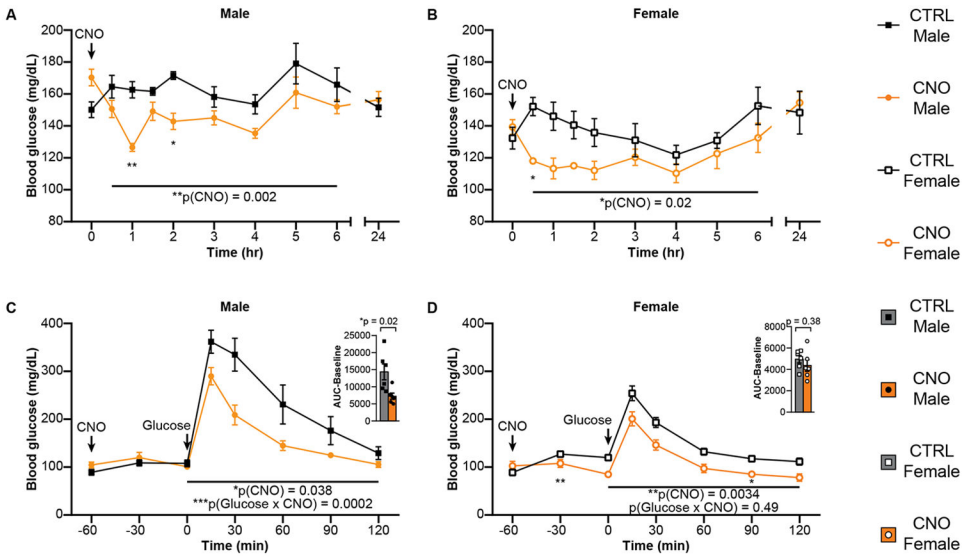

Fig. 4. Inhibition of δ cell activity decreases glycemia.

A and B) Hourly glucose measurements after administration of 1 mg/kg CNO at t = 0 min to A) male (n=6 CTRL, n=6 CNO) and B) female (n=6 CTRL, n=6 CNO) CNO-treated *Sst*-Cre x lsl-Gi-DREADD mice (CNO) or controls (CTRL). SAL-treated *Sst*-Cre x lsl-Gi-DREADD and CNO-treated *Sst*-Cre without lsl-Gi-DREADD mice were used as controls. C and D) GTT after 1 mg/kg CNO administration 1 hour before IP injection of glucose in male (C, n=6 CTRL, n=6 CNO) and female (D, n=6 CTRL, n=6 CNO) mice. Bar graphs in the upper right-hand corner of each line graph represent AUC-baseline. Significance was determined by two-way ANOVA for CNO (A, B) or glucose and CNO (C, D) followed by Holm-Sidak's correction for multiple comparisons (A: **p=0.0028, *p=0.010; B: *p=0.010; D: **p=0.0092, *p=0.031) and two-tailed unpaired t-test for AUC-baseline. Error bars represent SEM.

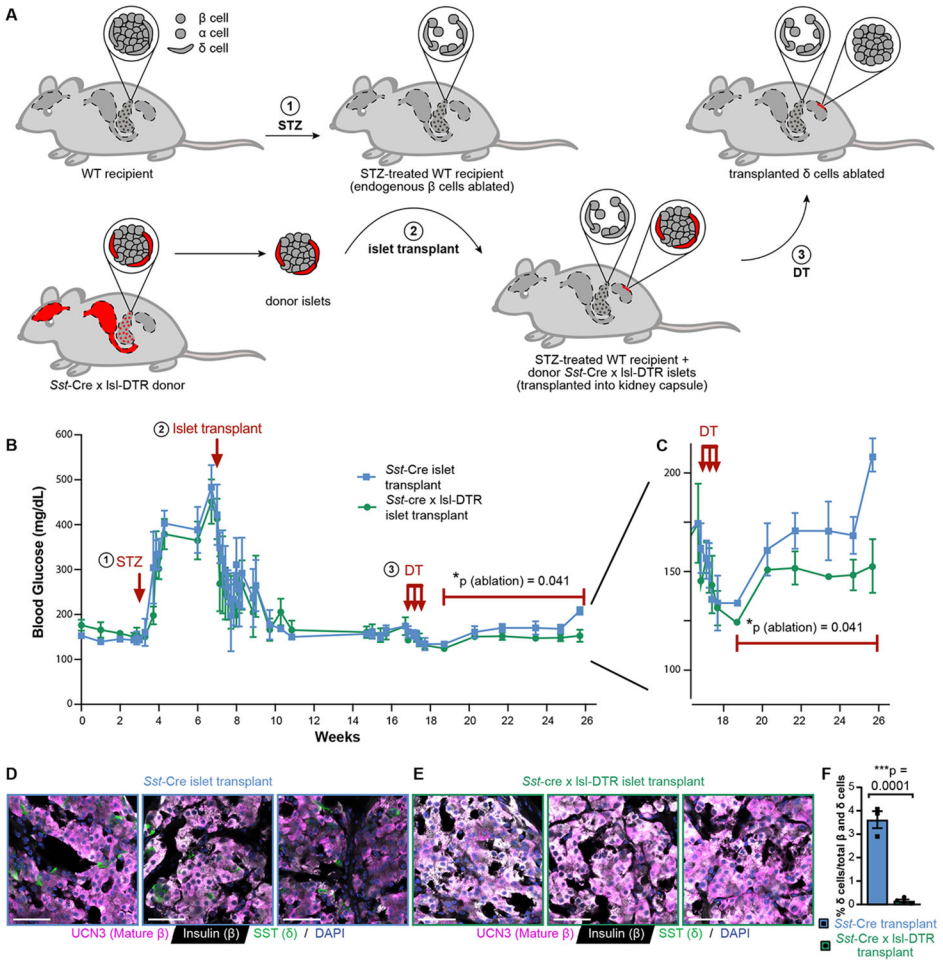

Fig. 5. Pancreatic δ cell ablation is sufficient to decrease the glycemic set point.

A) Schematic of the islet transplant strategy. 7 wild-type (WT) mice each received islets from a single donor (CTRL: n=3 WT receiving islets from *Sst*-Cre mice, DT: n=4 WT receiving islets from *Sst*-Cre x lsl-DTR mice). Outlines of the brain, stomach, gastrointestinal tract, pancreas, islets, and the kidney are shown within the mice. Red regions represent tissues in which DTR would be expressed in a *Sst*-Cre x lsl-DTR mouse. WT recipients were given 50 mg/kg of streptozotocin for 5 consecutive days (1). Islets were then isolated from *Sst*-Cre x lsl-DTR or control mouse donors and transplanted under the kidney capsule of the WT recipients (2). Only the δ within the transplanted islets express DTR in the recipient mice. After normoglycemia was re-established, the recipient mice with transplanted islets were administered 3 doses of DT as performed in the other experiments (3). B) Blood glucose measurements of the WT recipient mice throughout the course of the experiment. Blue lines represent recipients that received *Sst*-Cre islets (n=3) and green lines represent recipients that received *Sst*-Cre x lsl-DTR islets (n=4). C) An expanded view of the period during and after DT administration in B. D and E) Images of D) *Sst*-Cre only and E) *Sst*-Cre x lsl-DTR islets transplanted under the kidney capsule of WT mice. Scale bars represent 50 μm. F) Quantification of δ cells in *Sst*-Cre transplants (8,478 islet cells counted across n=3 mice) and *Sst*-Cre x lsl-DTR transplants (10,215 islet cells counted across n=4 mice). Significance was determined by two-way ANOVA for ablation followed

by Holm-Sidak's correction for multiple comparisons (B and C) and two-tailed unpaired t-test (F, ***p=0.0001). Error bars represent SEM.

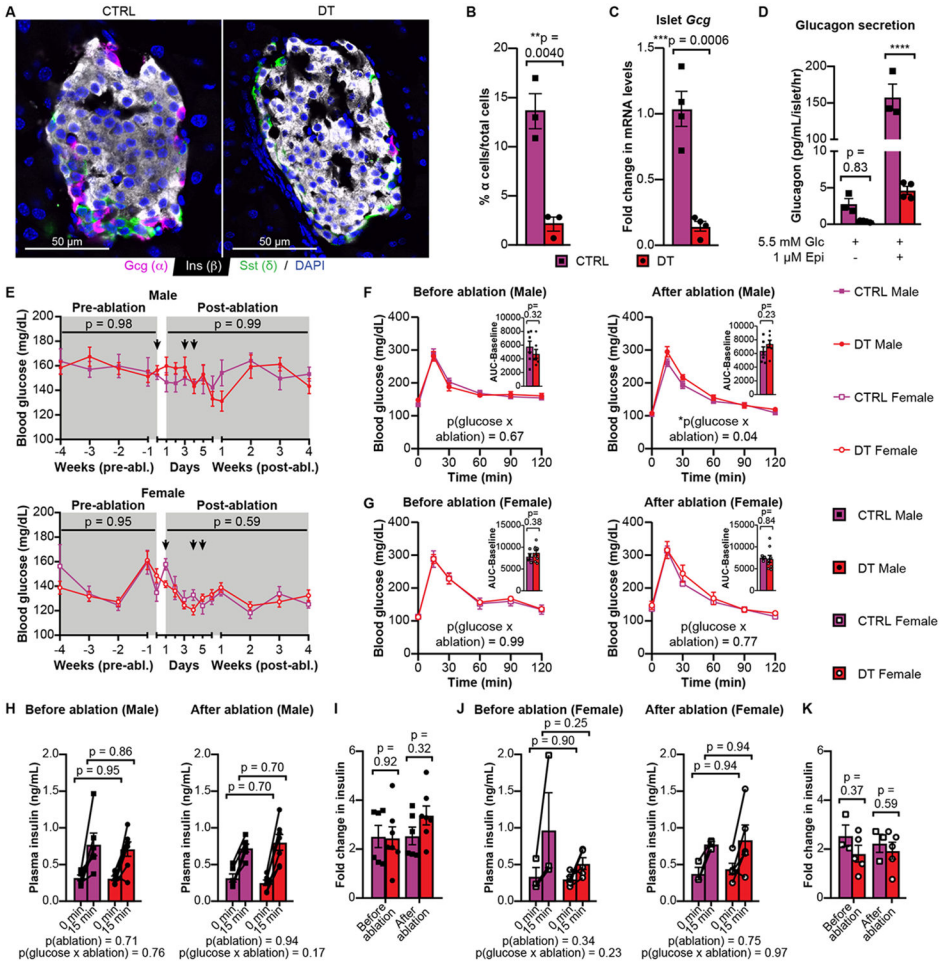

Fig. 6. α cell ablation does not affect basal glycemia.

A) Immunofluorescent stain of pancreas section from a non-ablated (left) and α cell-ablated mouse (right). Scale bar represents 50 μm. B) Quantification of α cell number (n=3 CTRL, n=3 DT). C) *Gcg* mRNA levels in islets from CTRL (n=4) and DT (n=4) mice. D) Glucagon secretion in CTRL (n=3 mice) and DT (n=4 mice) islets in the presence of 5.5 mM glucose +/− 1 μM epinephrine. E) Glucose measurements of male (top, n=5 CTRL, n=5 DT) and female mice (bottom, n=4 CTRL, n=10 DT). Arrows represent IP administration of DT. F and G) GTT in male (F, n=7 CTRL, n=7 DT) and female (G, n=4 CTRL, n=10 DT) mice before (left) and after (right) α cell ablation. Bar graphs in the upper right corner of each line graph represent AUC-baseline. H) Plasma insulin levels in male mice (n=6 CTRL, n=7 DT) before (left) and after (right) ablation. I) Fold change in plasma insulin levels between male CTRL and DT mice in H before and after administration of DT. J) Plasma insulin levels in female mice (n=3 CTRL, n=5 DT) before (left) and after (right) ablation. K) Fold change in plasma insulin levels between female CTRL and DT mice in J before and after administration of DT. Significance was determined by two-tailed unpaired t-test (B, C, AUC before and after ablation for F and G), two-way ANOVA for ablation and epinephrine (D, ****p<0.0001), ablation (E), or ablation and glucose (F-K) followed by Holm-Sidak's correction for multiple comparisons. Error bars represent SEM.

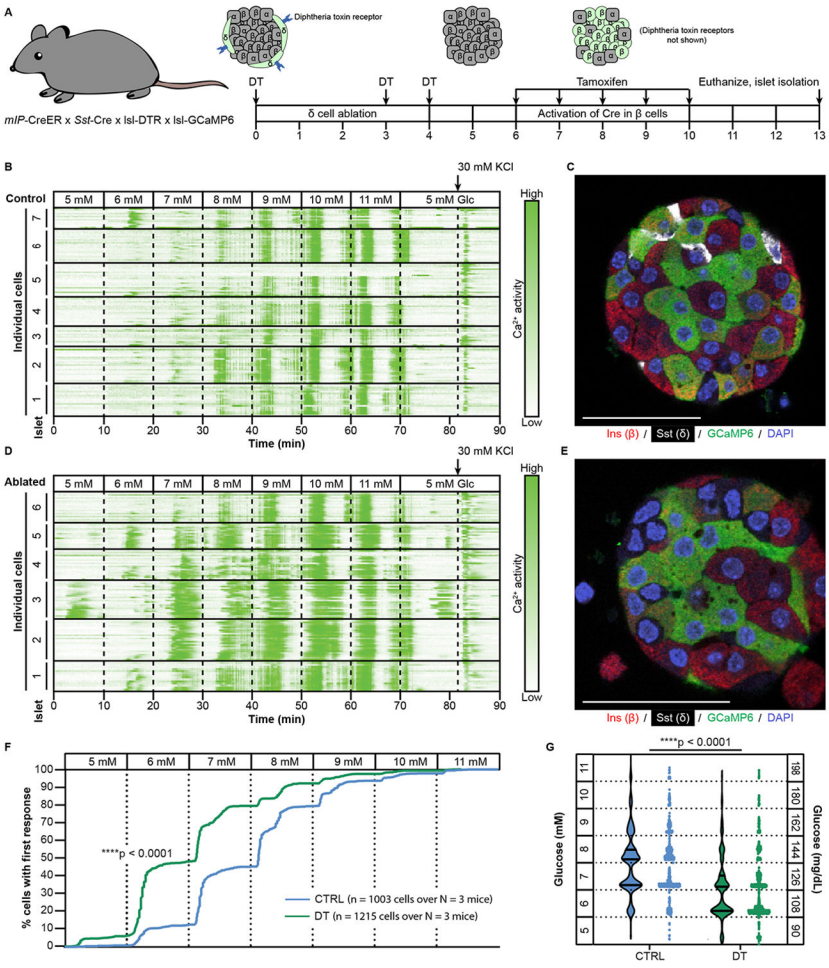

Fig. 7. β cells exhibit calcium response at a lower glucose threshold in the absence of δ cells.

A) Schematic of experimental design. B) Calcium traces from β cells in islets from a control mouse with intact pancreatic δ cells. C) *Post hoc* whole mount stain of an islet with intact δ cells. D) Calcium traces from β cells in islets from a mouse with ablated δ cells. E) *Post hoc* whole mount stain of an islet confirming absence of δ cells. Each line in panels B and D represents the calcium activity of a single β cell, with green intensity corresponding to an increase in intracellular calcium. Each box represents an islet. Dashed lines indicate the point at which the glucose levels were changed. Experiment was performed in n=3 mice (see Extended Data Fig. 5-7A). F) Curve representing the percentage that first respond at each glucose level. G) Violin plot in which each dot represents a cell and the glucose concentration to which it first responded. Significance was determined by Mantel-Cox test (F) and two-tailed unpaired t-test (G).

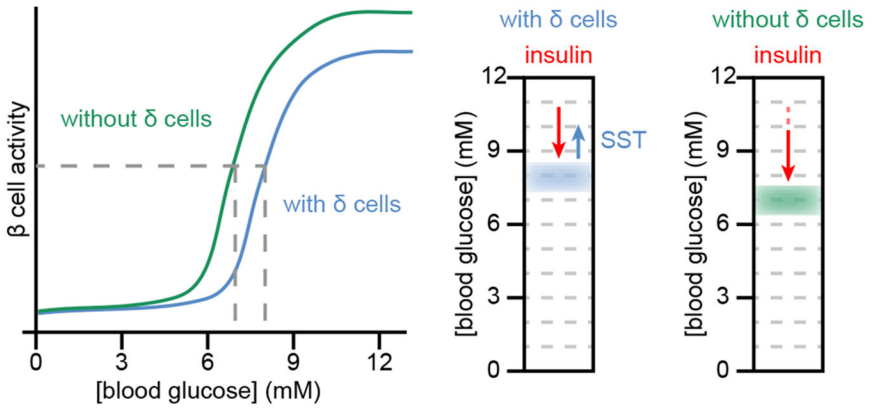

Fig. 8. Schematic of β cell glucose threshold and glycemic set point in the presence and absence of δ cells.

In the presence of δ cells, paracrine SST signaling pushes the β cell glucose threshold to the right, leading to a corresponding glycemic set point. When δ cells are removed, the absence of SST leads to a leftwards shift in the glucose threshold, leading to a corresponding decrease in the glycemic set point.